IOP Publishing Journal of Optics
J. Opt. 20 (2018) 075002 (9pp) https://doi.org/10.1088/2040-8986/aac748

Localized versus delocalized surface plasmons: dual nature of optical resonances on a silver circular wire and a silver tube of large diameter

Elena A Velichko[1] and **Denys M Natarov**[2]

[1] Department of Nonlinear Optics and Quantum Electronics, Institute of Radio-Physics and Electronics NASU, Kharkiv 61085, Ukraine
[2] Laboratory of Micro and Nano Optics, Institute of Radio-Physics and Electronics NASU, Kharkiv 61085, Ukraine

E-mail: elena.vel80@gmail.com

Received 5 March 2018, revised 7 May 2018
Accepted for publication 23 May 2018
Published 8 June 2018

Abstract

We investigate the resonances in the scattering and absorption of TE-polarized light by a solid circular silver wire and a silver tube larger than the wavelength radius and nanoscale thickness using the analytical solution and experimental data for the silver complex permittivity. We find that the resonances are well observed both in the visible and infra-red ranges if the scatterer radius is smaller than a certain value. They can be explained as the resonances on the standing surface-plasmon waves running along a curved metal-air interface or a metal layer, respectively. Still, each of them corresponds to one of the multipole localized surface plasmon modes of the circular wire or tube. This bridges the gap between localized and delocalized plasmons, which are complementary descriptions of the same physical effect intrinsic for metals in the visible range.

Keywords: scattering, localized surface plasmon resonance, sircular silver tube, circular silver wire

(Some figures may appear in colour only in the online journal)

1. Introduction

Plasmonics is a branch of today's photonics, which is closely associated with nanophysics and the nanotechnology of noble-metal particles of sizes usually ranging from 10 nm to 100 nm. Such particles are famous for the localized surface plasmon (LSP) resonances in the visible range. Similar resonances are demonstrated by the noble-metal nanowires of the same diameters shaped as elongated rods with a fixed cross-section. Numerous textbooks on optics and nanotechnologies (e.g. see [1]) explain that the LSP resonance wavelength for a spherical particle with the relative dielectric permittivity of metal ε_M : Re $\varepsilon_M < 0$ in the air satisfies the equation $\mathrm{Re}\varepsilon_M(\lambda) = -2$, and for a infinite solid circular metal nanowire, a similar equation is $\mathrm{Re}\varepsilon_M(\lambda) = -1$. According to the well established experimental data of [2], for the silver wire, the wavelength, which satisfies the textbook equation, is in the ultraviolet band at $\lambda = 337$ nm; we will call this value, for brevity, 'the textbook LSP wavelength'.

Such a common description of LSP resonance implies that the circular metal nanowire has only one LSP resonance. Indeed, the experiments show that the spectrum of the total scattering cross-section or the extinction cross-section of a silver wire demonstrate a single broad peak around the textbook wavelength. As optical resonances are associated with the natural modes of the scatterer, this may give the impression that the underlying LSP mode is also only one. However, accurate modelling with the aid of the method of separation of variables applied to the Maxwell equations (see [3]) shows that there exists an infinite number of independent LSP modes

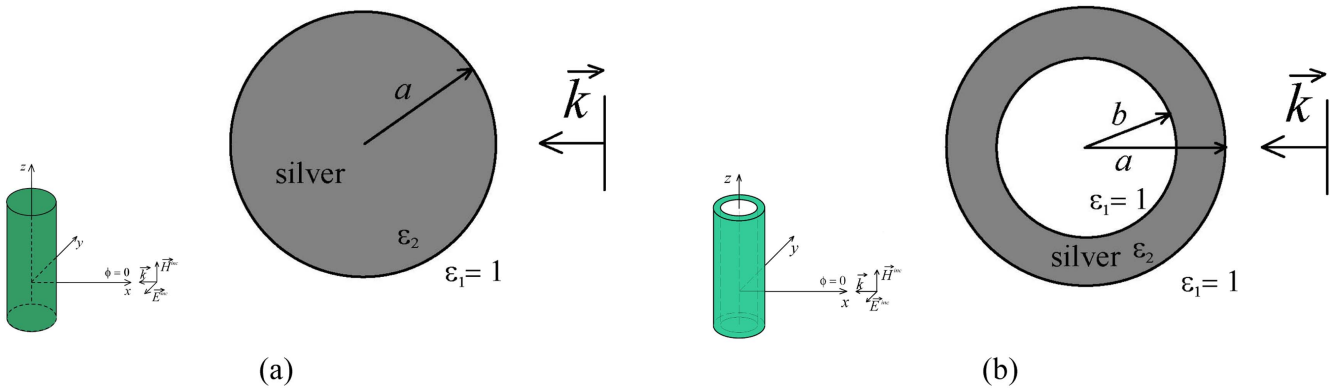

Figure 1. General view and cross-sectional geometry of a solid circular silver wire (a) and a circular silver tube (b).

associated with complex poles of all azimuthal orders $m = 1$, 2, ... of the scattered optical field. Such an analysis also shows that the shift of the actual mth LSP resonance wavelength from the textbook value is proportional to $(1/m)(a/\lambda)^2$. Thus, if $a \ll \lambda$, the maximum shift is observed for the 'dipole' plasmon mode associated with $m = 1$, however all the shifts are very small. Besides that, the bulk losses in metals are sizable near the textbook LSP wavelength where the $\mathrm{Im}\varepsilon_M$ of silver varies around 0.3. This leads to the effect that the resonances on all LSP modes in the spectra of both the scattering and absorption of light by a deep sub-wavelength wire merge together into a single broad peak at $\lambda \approx 340$ nm [1, 3].

On the other hand, if a silver wire becomes highly super-wavelength, $a \gg \lambda$ (say, $a = 1$ mm that is over 1000λ in the visible range) then everyday experience tells us that the scattering of light is reduced to purely geometrical-optics effects and no resonances are observed.

In general, the resonances on the first few higher-order multipole LSP modes on a several hundred nanometre and smaller particles are well documented theoretically [3–7] and even measured experimentally [8–10]. Here, only [7] addressed the LSP modes on a metal particle, which was moderately larger than the wavelength, however still far from being treatable with geometrical optics. Still in [7], the particle was a spherical one and the LSP modes were studied as solutions to the eigenvalue problem without a direct link to the scattering. It looks like there is no published study, either in textbooks or in research papers, on the transverse LSP resonances on a similarly large metal wire. In particular, it is not clear how large a solid metal wire radius can be used to demonstrate the LSP resonances.

Besides, one can make a statement that the resonances on multipole LSP modes of a metal wire could only be observed if a wire were made of metal with $\mathrm{Im}\varepsilon_M < 0.001$ [4]. This level of loss is not realistic in the visible range, however it seems that such a statement is too restrictive.

Besides solid wires, even more intensive transverse LSP resonances are known in the scattering and absorption of light by noble-metal tubes having nanoscale thickness [11–17]. Such nanotubes are commonly used in optical sensors [18, 19]. This is because the LSP modes on the tube outer and inner boundaries show hybridization and some of them obtain considerably red-shifted wavelengths compared to the solid nanowire [11, 16]. Thanks to that, they get to the yellow and even the red part of the visible spectrum where the bulk losses in metals are lower than in the violet part. The shift depends on tube's thickness, and the above formulated question about the maximum radius of the metal tube to observe the hybrid LSP (HLSP) resonance is equally interesting.

The study presented below is aimed at obtaining answers to the abovementioned questions. Some of the initial results related to a solid wire were reported in the conference paper [20]. Here, they are presented in a more complete form and extended to the study of the larger-than-wavelength tube scattering. In the remainder, we present basic field expressions and then discuss in detail the scattering by a solid silver wire that is followed by a similar study for a silver tube.

2. Scattering problem solution

We assume that an H-polarized plane wave with the harmonic time dependence $\exp(+i\omega t)$ (where ω is the cyclic frequency) is incident, normally to its axis, on a solid circular silver cylinder with radius a or a tube with the outer radii a and the inner radius b, so that $h = a–b$ is the tube thickness (see figure 1).

To characterize the electromagnetic field, we introduce cylindrical coordinates (r, φ, z) with the axis z being the cylinder or tube axis. The objects are placed in vacuum and the electromagnetic field is assumed not depending on z. This means that the considered scattering problem is two-dimensional (2D) and can be analyzed with the aid of the magnetic field z-component $H_z(\vec{r})$ where $\vec{r} = (r, \varphi)$. The electric field components $E_r(\vec{r})$ and $E_\varphi(\vec{r})$ are found from $H_z(\vec{r})$ using the Maxwell equations. The function H_z must satisfy the Helmholtz equation, the continuity conditions for the field tangential components at each boundary ($r = a$ for solid wire and $r = a$, b for tube), the condition of the local power finiteness, and the scattered field must satisfy the Sommerfeld radiation condition. Combined together, these conditions guarantee the uniqueness of the problem solution.

The incident plane wave is expressed as

$$H_z^{inc}(r, \varphi) = \exp(ikx), \tag{1}$$

where $x = r\cos\varphi$, $y = r\sin\varphi$, and $k = \omega/c = 2\pi/\lambda$ is the free-space wavenumber while c is the light velocity and λ is the free-space wavelength.

The circular shape of the boundaries between different materials suggests the use of the method of separation of variables [21]. This means we expand both the incident field, the scattered field (in the outer domain), and the field inside the inner domains of the wire or tube in terms of the Fourier series in the angular coordinate φ. Then the boundary and other conditions lead to the following explicit expressions for the tube:

$$H_z(r,\,\varphi) = \sum_{m=0}^{\infty} \delta_m i^m T_{1m} J_m(kr)\cos m\varphi, \quad r < b \tag{2}$$

$$H_z(r,\,\varphi) = \sum_{m=0}^{\infty} \delta_m i^m [T_{2m} J_m(\nu kr) + R_{2m} H_m^{(2)}(\nu kr)] \times \cos m\varphi,\ b < r < a, \tag{3}$$

$$H_z(r,\,\varphi) = H_z^{inc}(r,\,\varphi) + \sum_{m=0}^{\infty} \delta_m i^m R_{3m} H_m^{(2)}(kr), \quad r > a, \tag{4}$$

where $\delta_m = 1$ if $m = 0$ and 2 otherwise, and the coefficients are

$$T_{1m} = \frac{4(\nu\pi k)^{-2}(abD_m)^{-1}}{J_m(kb)H_m^{(2)'}(\nu kb) - \nu J_m'(kb)H_m^{(2)}(\nu kb)}, \tag{5}$$

$$T_{2m} = 2i(\pi kaD_m)^{-1}, \quad R_{2m} = 2iP_m(\pi kaD_m)^{-1}, \tag{6}$$

$$R_{3m} = [\nu J_m'(ka)(J_m(\nu ka) + H_m^{(2)}(\nu ka)P_m) - J_m(ka)(J_m'(\nu ka) + H_m^{(2)'}(\nu ka)P_m)]D_m^{-1}, \tag{7}$$

$$D_m = H_m^{(2)}(ka)(J_m'(\nu ka) + H_m^{(2)'}(\nu ka)P_m) - \nu H_m^{(2)'}(ka) \times (J_m(\nu ka) + H_m^{(2)}(\nu ka)P_m), \tag{8}$$

$$P_m = \frac{\nu J_m'(kb)J_m(\nu kb) - J_m(kb)J_m'(\nu kb)}{J_m(kb)H_m^{(2)'}(\nu kb) - \nu J_m'(kb)H_m^{(2)}(\nu kb)}. \tag{9}$$

Here, $k_M = \nu k$ is the in-metal wavenumber, $\nu = \nu_M = \varepsilon_M^{-1/2}$ is the metal refractive index, $\varepsilon_M = \varepsilon_M(\lambda)$ is the wavelength-dependent complex relative dielectric permittivity of metal, $J_m(\cdot)$ and $H_m^{(2)}(\cdot)$ are the Bessel and Hankel functions, respectively, and the prime means the differentiation in the argument. These functions can be easily computed to machine precision; hence the accuracy of determining the field is controlled by the upper limit of summation in (2)–(4). Therefore, the obtained results are numerically exact and can serve as reference data.

The case of the solid wire can be obtained from (5)–(9) after passing to the limit of $b \to 0$; note that then $P_m = T_{1m} = R_{2m} = 0$.

As usual, the considered lossy scatterers will be characterized with their total scattering and absorption cross-sections (TSCS and ACS),

$$\sigma_{sc} = \frac{4}{k}\sum_{m=0}^{\infty} \delta_m |R_{3m}|^2,$$
$$\sigma_{abs} = -\frac{4}{k}\,\mathrm{Re}\sum_{m=0}^{\infty} (-1)^m \delta_m R_{3m} - \sigma_{sc} \tag{10}$$

Presented further results for the quantities (10) are normalized by $4a$, which is the limit value of σ_{sc} at $a/\lambda \to \infty$.

3. Numerical results

3.1. Dielectric function of silver

In computations, we do not use the Drude formula for the dielectric function of silver, because it provides grossly incorrect values of Re $\varepsilon_M(\lambda)$ and especially Im $\varepsilon_M(\lambda)$ in the violet range where all LSP modes of the solid silver wire and some of the hybrid LSP modes of the circular silver nanotube are located (see e.g. [16–18]). Instead, we take the experimental data of Johnson and Christy [2], widely recognized as reliable [22], and use the Akima spline interpolation algorithm to obtain ε_M (λ) at any λ. This cubic-spline technique generates the curves that take exactly the values tabulated in [2], however are continuous and have a continuous derivative in λ. For clarity, we show these curves in figure 2, together with the Drude approximation, which is plotted for the static permittivity 1.445, plasma cyclic frequency 13 280 THz and damping constant 91.3 THz.

Note also that, according to [8, 12], the non-local effects in a metal wire or tube scattering must be taken into account only if a or $h < 5$ nm, respectively. Besides, the approximate effect of size can be accounted for empirically like it was done in [7] for a spherical particle. This leads to small changes in Reε_M (λ) and somewhat larger values of Imε_M (λ).

3.2. Solid silver wire

In figure 3, we present the plots of the normalized TSCS and ACS as a function of the wavelength in the visible range, for silver cylinders of small (50 nm) and large (500 nm) radii. The collective peak on the LSP modes is well observable in both cases in the scattering and only for $a = 50$ nm in the absorption. If $a \leqslant 50$ nm, the TSCS and ACS peaks are at the ultraviolet wavelength very close to textbook value of 337 nm. However for $a = 500$ nm the peak in the scattering is sizably red shifted and in addition is modulated by a collection of several distinct small peaks.

Therefore, two questions appear, at least: (i) what is the nature of these smaller peaks and (ii) why the main peak is red-shifted? The answers to these questions appear if we look at the TSCS and ACS as functions of two variables, the wavelength and the wire radius.

In figure 4, we present the corresponding maps of the normalized TSCS and ACS. In the inserts, we show a zoomed domain, in the lower part of which the 'sub-wavelength rule' Re$\varepsilon_M(\lambda) = -1$ (shown by white vertical dashed line) is valid. Here, we can see the fine structure of multiple TSCS and ACS

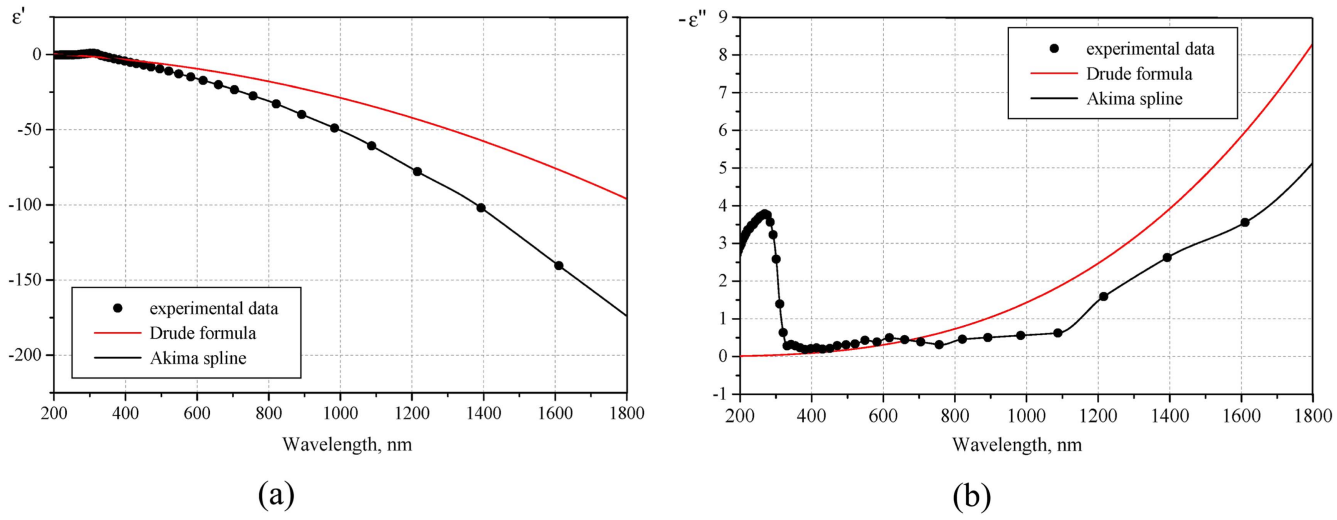

Figure 2. Real (a) and imaginary (b) parts of the dielectric function of bulk silver versus the wavelength: comparison of experimental data of [2] and Drude formula.

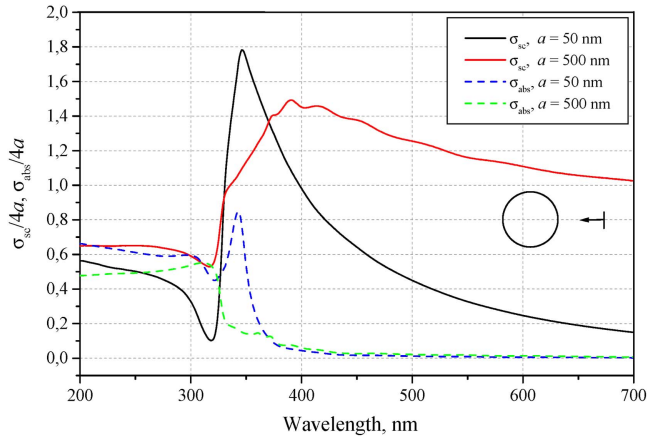

Figure 3. Normalized by $4a$ TSCS and ACS of a solid silver wire as a function of the wavelength, for several values of the radius a.

resonances on the right side from the $\lambda = 337$ nm value, well visible for all $a \geqslant 20$ nm. They form a sort of locally periodic, in a, 'ridges' on the maps of TSCS and ACS, even if $a = 1000$ nm or larger.

In figure 5, the map of the normalized by $4a$ ACS is additionally normalized by the wavelength-dependent factor $\mathrm{Im}\varepsilon_M(\lambda)$, to remove the effect of bulk losses in silver that grow up sharply in the ultraviolet (this appears as green area in figure 4(b) to the left of 337 nm). Note the vertical 'ridge' at $\lambda = 325$ nm, which keeps its shape for any radius larger than 50 nm. According to measurements [2], at this wavelength for silver $\mathrm{Re}\varepsilon_M = 0$ and $\mathrm{Im}\varepsilon_M = 0.4$. After additional normalization, the separate resonances are even more visible. We are going to show that they are associated with the minima of the functions $|D_m|$ (with $m = 1, 2, \ldots$), i.e. with the multipole LSP modes.

To this end, we present in figure 6, the relief of $|D_1|$ as a function of the wavelength and the radius of a cylinder, i.e. expression (8) for $b = 0$ and $m = 1$.

As one can see, there are two deep minima of $|D_1|$ near $\lambda = 340$ nm and 325 nm. The minimum near 325 nm corresponds to a 'secondary plasmon mode' that can be revealed if a modified Drude description of silver is used—see [23] for details. Such a mode does not show up as a peak in figure 3 because of large bulk losses in the ultraviolet. However, the minimum at 340 nm corresponds to the conventional localized SP mode of the dipole type. The reliefs of $|D_m|$ for $m > 1$ look very similar.

Note that, when studying the resonances on a solid wire of the radius larger than 30 nm, we cannot use the quasi-static approximate equations for D_m with $m > 1$ based on the small-argument asymptotics of the Bessel functions. This becomes evident if we visualize the domain where $ka \leqslant 1$, $|k_M a| \leqslant 1$—see dashed lines in figure 6. It is only the minimum of $|D_1|$ that is found there. Indeed, it can be satisfactorily found from quasi-static equation derived in [3], $D_1 = const\tilde{D}_1 = 0$,

$$\tilde{D}_1 \approx \varepsilon_M(\lambda) + 1 - \frac{\pi^2}{2}\left(\frac{a}{\lambda}\right)^2 [\varepsilon_M(\lambda) - 1] \times \left[2 + \varepsilon_M(\lambda) - 4\ln\frac{\pi\gamma a}{\lambda}\right]. \quad (11)$$

In figure 7, we present the map of the normalized ACS overlapped with the lines of the minimum values of $|D_m|$ for indices $m = 1, 2, 3, 4$ and 5. As one can see, the maxima of ACS coincide with the minima of $|D_m|$.

To reveal the underlying physics of the resonance behaviour of a solid circular wire with larger-than-wavelength radius, we plot in figure 8 the normalized ACS as a function of the radius, calculated at fixed wavelengths. As one can see, for large a the distances in a between two adjacent peaks are 49.5 nm at $\lambda = 375$ nm. This corresponds to the arc length value of 311 nm.

Now we can compare this value with the wavelength of the SP wave on a flat infinite interface between the silver and the free space. An analytical expression for this wavelength

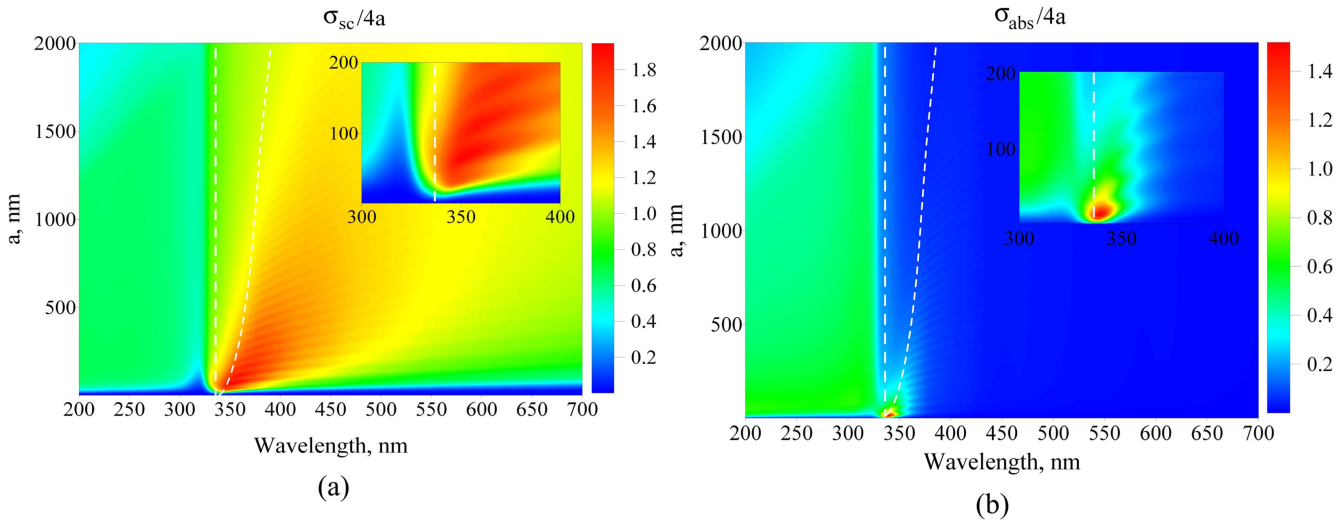

Figure 4. Maps of the normalized by 4*a* TSCS (a) and ACS (b) of a solid silver wire, as a function of the wavelength and the radius.

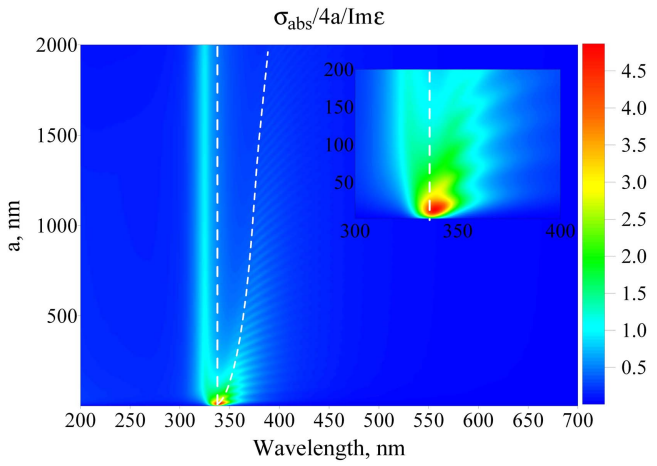

Figure 5. Map of the normalized by 4*a* and the factor Im $\varepsilon_M(\lambda)$ ACS of a solid silver wire, as a function of the wavelength and the radius.

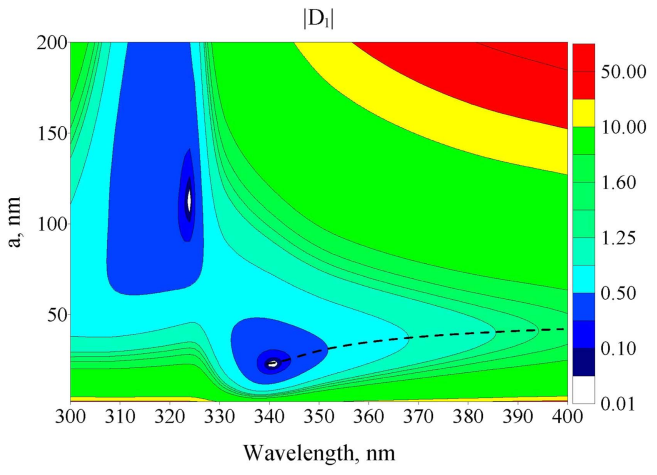

Figure 6. Map of $|D_m|$ as a function of the wavelength and the radius of a silver wire, for $m = 1$; black dashed line shows the minima at fixed λ.

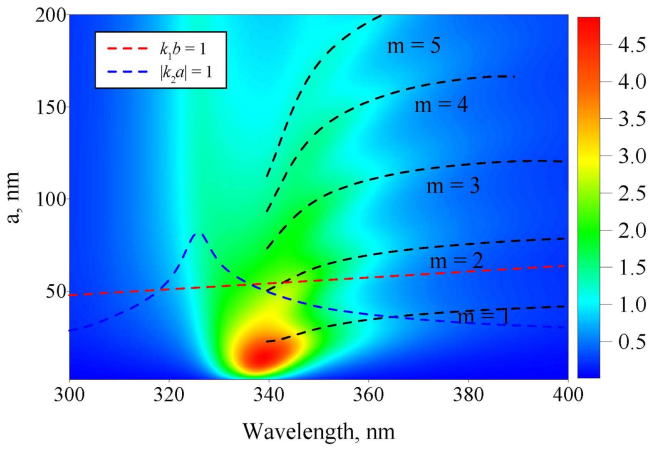

Figure 7. Map of ACS of a nanosize silver cylinder normalized by 4*a* Im ε_M (λ) (same as the inset in figure 4), overlapped with the curves $ka = 1$ (red dashed line) and $ka|\nu_M| = 1$ (blue dashed line); black dashed lines indicate the minima of $|D_m|$ for different values of index m.

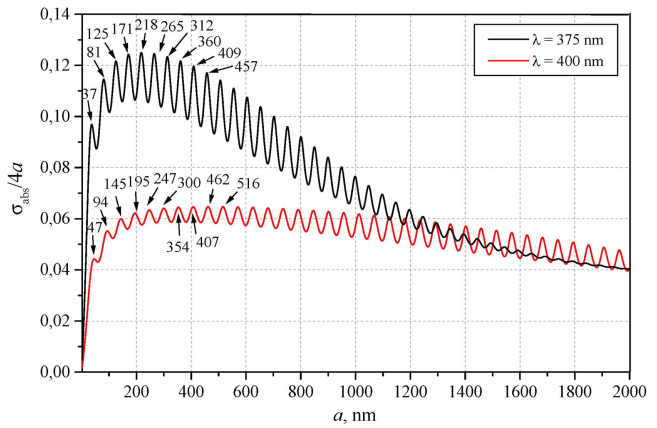

Figure 8. The normalized ACS of a silver cylinder as a function of its radius.

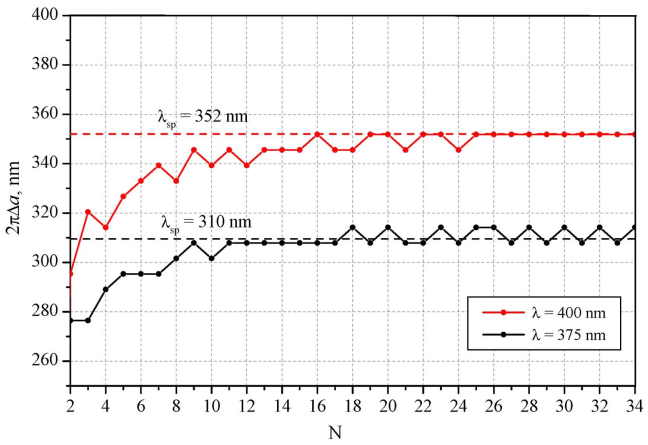

Figure 9. The distances between adjacent values of wire's circumference corresponding to the maxima of ACS in figure 7 versus the number of the maximum.

can be found in [1], where we denoted $\varepsilon_M = \varepsilon'_M - i\varepsilon''_M$.

$$\gamma'_{sp} = k\,\mathrm{Re}\left[\frac{\varepsilon_M(\lambda)}{\varepsilon_M(\lambda)+1}\right]^{1/2} = k\left[\frac{\varepsilon'_M(\lambda)}{\varepsilon'_M(\lambda)+1}\right]^{1/2} + k\,O(\varepsilon''^2_M) > k. \tag{12}$$

In figure 9, we show the dependences of the inter-peak distances in terms of the arc length on the peak's number, counted from the small radii. The dashed lines are the values of $\lambda_{sp}(\lambda) = 2\pi/\gamma'_{SP}$ calculated from (12) using the data of [2]. As one can see, as soon as a silver wire's circumference approaches $10\lambda_{sp}$, the resonances can be interpreted, with a few per cent accuracy, as consecutive resonances of the SP wave (12) running around the cylinder. Note that each of them can be still interpreted via the mth order multipole LSP mode that is the root of $D_m(\lambda, a) = 0$.

In figures 10(a)–(c), we show the magnetic field patterns computed in the ACS maxima for silver wires with four different radii at the fixed wavelength of $\lambda = 375$ nm (black curve in figure 7). These patterns demonstrate clear standing-wave portraits corresponding to the LSP modes: the dipole mode P_1 (a), and the multipole modes P_{13} ($m = 13$) (b) and P_{21} ($m = 21$) (c).

In contrast, there is no standing wave pattern in figure 10(d) for the wire of the 2000 nm radius. This is because the in-shadow part of wire's surface, i.e. its half-circumference, is considerably larger than the propagation distance of the SP wave on the infinite interface between silver and free space. This distance is defined as $l_{SP} = \gamma''^{-1}_{SP}$, where

$$\gamma''_{SP} = k\,\mathrm{Im}\left[\frac{\varepsilon_M(\lambda)}{\varepsilon_M(\lambda)+1}\right]^{1/2} = k\frac{\varepsilon''_M(\lambda)}{2\varepsilon'^{1/2}_M(\lambda)[\varepsilon'_M(\lambda)+1]^{3/2}} + kO(\varepsilon''^2_M) < k. \tag{13}$$

Plotting the value $a_{\mathrm{lim}} = l_{SP}/\pi$ on the colour maps in figures 4 and 5 (white dashed curves) yields a parabola, $a_{\mathrm{lim}} = const \cdot \lambda^2$, above which the resonances on the multipole LSP modes are not observed. This is fully in line with common sense: on large metal scatterers, only GO effects are present in the visible light—now it is clear why.

3.3. Silver tube

In figure 11, we show the spectral dependences of TSCS and ACS in the visible range for three silver tubes of small (60 nm) and large (510 nm and 1010 nm) values of the outer radius. The tube thickness is kept the same, $h = 10$ nm. As mentioned in the introduction, if h is smaller than the skin-depth for silver in the optical range (that is 10 to 20 nm), then a thin silver nanotube displays the hybridization of the LSP modes of the inner and outer boundaries [11, 16]. Two peaks on the dipole-type HLSP modes P_1^+ and P_1^- are well observable, both on the TSCS and ACS plots for a 10 nm thin tube of $a = 60$ nm. If a becomes smaller, then the TSCS and ACS peaks shift closer to the textbook LSP wavelength of 337 nm predicted by the 'sub-wavelength rule' $\mathrm{Re}\varepsilon_M(\lambda) = -1$ for a solid silver nanowire. However, for the larger values of a the peaks in the scattering and absorption get sizably red-shifted and split.

Similar to the analysis of solid wire scattering, we can try to clarify the resonances by studying TSCS and ACS as functions of two parameters, namely the wavelength and the tube outer radius. In figure 12, we present the corresponding maps of the normalized TSCS and ACS.

On the maps, we can see the fine structure of multiple TSCS and ACS resonances. They form a sort of locally periodic, in a, 'ridges' stretching far beyond $a \geqslant 1000$ nm and $\lambda \geqslant 1000$ nm, and each of them corresponds to a multipole hybrid LSP mode P_m^-, $m = 1, 2, 3, \ldots$. Note the darkened vertical strips of lower absorption in figure 12(b) that correspond to the local minima of bulk losses in silver at 800 nm and 1100 nm [2].

To visualize the resonance behaviour of ACS of a circular silver tube with large radius, we plot in figure 13 the normalized ACS as a function of the outer radius, at the fixed wavelengths of 600 nm and 800 nm.

One can see periodic sequences of HLSP peaks until radius a does not exceed a certain value, different to each wavelength. Similar to our analysis of a solid wire scattering, we can compare the inter-peak distances with the wavelength of the SP wave on a thin flat metal layer.

This needs a more careful analysis as a metal layer can support not one but two hybrid SP (HSP) waves, long-range and short-range. The long-range HSP wave was studied in detail in [24] in view of its application in power transfer. However, in the scattering by nanoshells it happens that the resonances are related to the other HSP wave, the short-range one. Note that the short-range HSP wave is the same wave,

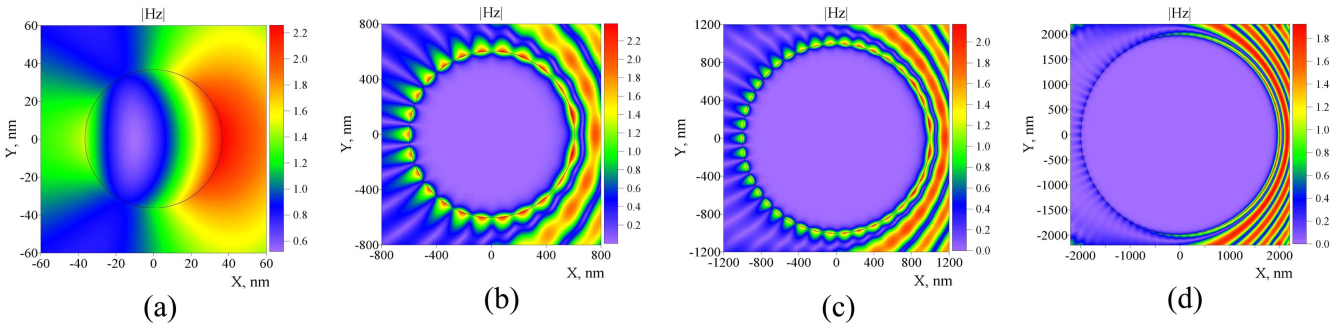

Figure 10. The near-zone magnetic field patterns in the ACS maxima for the silver wires with radii $a = 37$ nm (a), 604 nm (b), 998 nm (c), and 2000 nm (d), all at the wavelength $\lambda = 375$ nm.

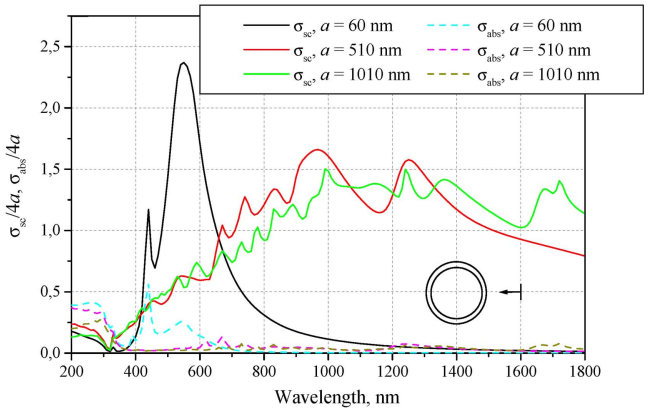

Figure 11. Normalized by $4a$ TSCS and ACS of a silver tube as a function of the wavelength, for several values of the outer radius a.

which is responsible for the Fabry–Perot-like LSP resonances on finite flat silver strips [25, 26].

Indeed, using the accurate dispersion equation for that mode, shown as equation (15) in [24], and assuming that $h \to 0$, $\gamma_{SP} = \gamma'_{HSP} - i\gamma''_{HSP}$, we get

$$\gamma'_{HSP^-} \approx k\{1 + 4[\varepsilon'_M(\lambda)kh]^{-2}\}^{1/2} \gg k. \qquad (14)$$

In figure 14, we show the dependences of the inter-peak distances (in terms of the arc length) on the peak's number, counted from the small radii. The dashed straight lines are the values of $\lambda_{sp}(\lambda) = 2\pi/\gamma'_{HSP^-}$ calculated using (14) for the flat silver layer of 10 nm thickness.

As one can see, as soon as the silver tube's circumference approaches $5\lambda_{sp}(\lambda)$, the hybrid LSP resonances P_m^- can be also interpreted as consecutive resonances of the short-range HSP wave running around the tube. Still, in our case each resonance can be also interpreted via a root of characteristic equation $D_m(\lambda, a) = 0$, see (8).

To support our interpretation, we present in figure 15 the magnetic field patterns in the ACS maxima for a silver tube at the wavelength fixed at 600 nm and the tube thickness taken as $h = 10$ nm (red curve in figure 13).

The near magnetic field in the resonances is dominated by the contribution from the corresponding multipole HLSP mode. They are well recognizable in these patterns as they demonstrate bright spots, which stick to the boundaries of the tube. Zero magnetic field at the middle circumference of the tube can be also seen (especially in figures 15(a)–(e)), as expected for the 'difference' HLSP modes. Note that, unlike the solid wire case presented in figure 9, the light penetrates through the 10 nm thin wall and reaches the inner void space. Moreover, figures 15(h)–(j) demonstrate that the HLSP modes on such a thin tube of the radius larger than 500 nm can further hybridize with the modes of the inner void of the tube. This is revealed by the appearance of bright spots of magnetic field *inside* the void, i.e. not sticking to its inner boundary.

The near field patterns in figure 15 are presented for a thin-wall tube. Actually, the 10 nm thickness here is smaller that the skin depth for silver (around 20 nm in the optical range). Therefore, the wall is partially transparent, which enables the electromagnetic wave to reach the inner void and hence leads to the LSP hybridization. In the case of thicker than 100 nm walls, the hybridization ceases and the LSP modes of the inner boundary are not excited; the tube in this case scatters and absorbs the plane wave very similarly to a solid wire. The corresponding plots of TSCS and ACS of such thick tubes show only one peak associated with the LSP modes of the outer boundary—see [27].

Further, similar to the case of solid metal wire, we introduce the *propagation distance* $l_{SP} = \gamma''^{-1}_{HSP}$ of the short-range HSP wave on the flat silver film of thickness h, where the adequate expression for γ''_{HSP} is found from equation (15) of [24],

$$\gamma''_{HSP} \approx 2\varepsilon''_M(\lambda)[\varepsilon'^2_M(\lambda)h]^{-1} < k. \qquad (15)$$

The white dashed curves in figure 11 show the value $a_{\lim} = l_{SP}/\pi$ and indicate the approximate limit size of the tube outer radius beyond which the HLSP wave, while travelling to the opposite side of the shadow part of the tube, decays too much to form a standing wave. Similar to the solid wire, for a thin tube such a curve is shaped roughly as a parabola, $a_{\lim} \approx \text{const} \cdot \lambda^2 h$; above that curve, the resonances on the multipole hybrid LSP modes are poorly observable.

A new feature with respect to the solid metal wire is the almost linear dependence of $a_{\lim}$ on the tube thickness h: the thinner the tube, the shorter the propagation distance. However, approximate expression (15) is valid only for thin metal layers ($kh \ll 1$) and if h becomes larger, then the complex

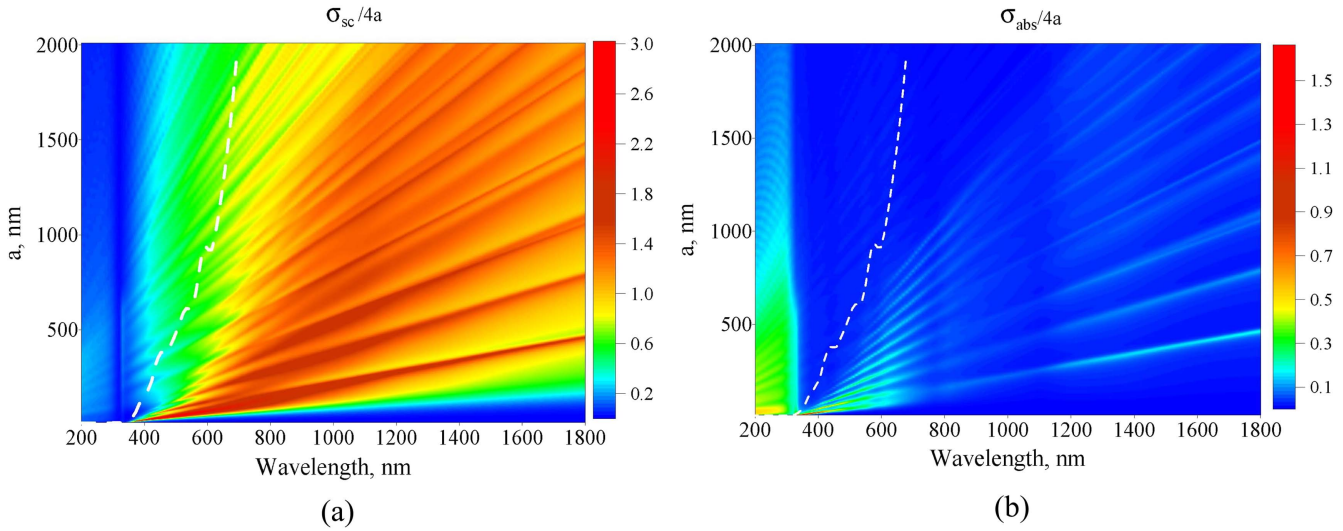

Figure 12. Maps of the normalized by $4a$ TSCS (a) and ACS (b) of a silver tube, as a function of the wavelength and the outer radius, with the thickness of tube being fixed at 10 nm.

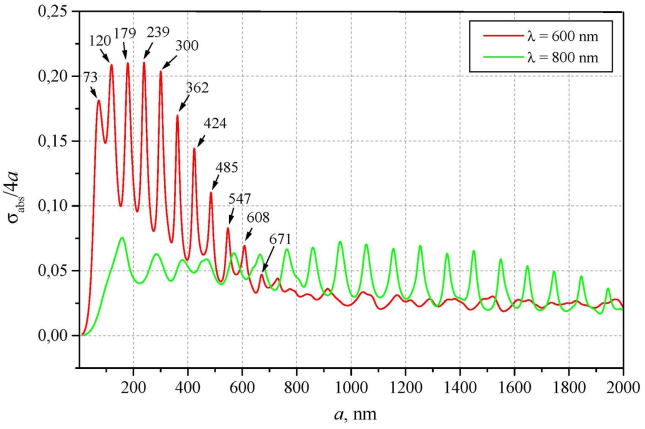

Figure 13. The normalized ACS of a silver tube as a function of its radius.

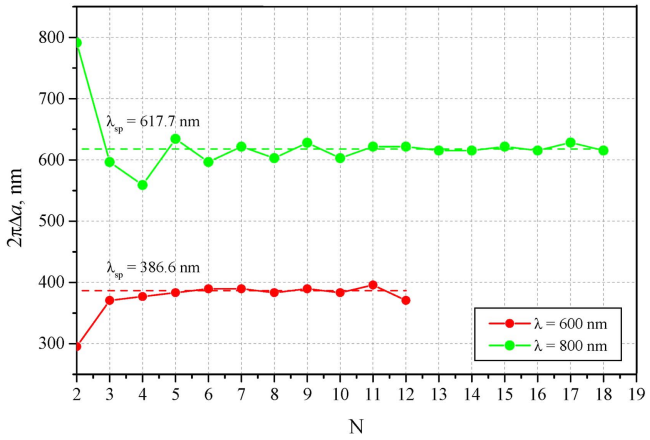

Figure 14. The distances between adjacent values of tube circumference corresponding to maxima of ACS in figure 12.

value of $\gamma_{HSP} = \gamma'_{HSP} + i\gamma''_{HSP}$ should be found as a solution of the full characteristic equation; see [24].

4. Conclusions

We have considered the scattering and absorption of the TE-polarized plane wave by a circular solid metal wire and silver tube of the radius comparable or larger than the wavelength, in the visible and infra-red ranges. Each resonance can be explained in two ways: (i) as a standing wave formed by the pair of oppositely traveling delocalized SP-waves and (ii) as a resonance on the localized SP mode of the azimuthal order $m > 0$.

We have demonstrated that, in contrast to widespread opinion that LSP resonances in visible light scattering and absorption by metal scatterers are associated with nanosize particles and wires, they can be clearly observed on much larger metal objects. They have dualistic nature: on the one side, they can be understood as short-range SP-wave resonances (standing waves) around the whole scatterer's surface. On the other hand, each of them can still be associated with a certain azimuth order of the electromagnetic field in the presence of such a scatterer. Only if the part of the scatterer outer boundary that is in shadow considerably exceeds the propagation length of the SP wave (which grows with the free-space wavelength, however is still finite, in dozens and small hundreds of λ), then these resonances cease to be observable.

All of the above should remain qualitatively valid if a metal scatterer cross-section is not a circle but still has a smooth boundary. If, contrary, it is has sharp bends (say as a polygon) then the standing-wave LSP resonances are formed between the adjacent bends. Therefore, to have them observable, the smooth parts of the boundary must be not much longer than the corresponding propagation distance of the SP or short-range HSP wave.

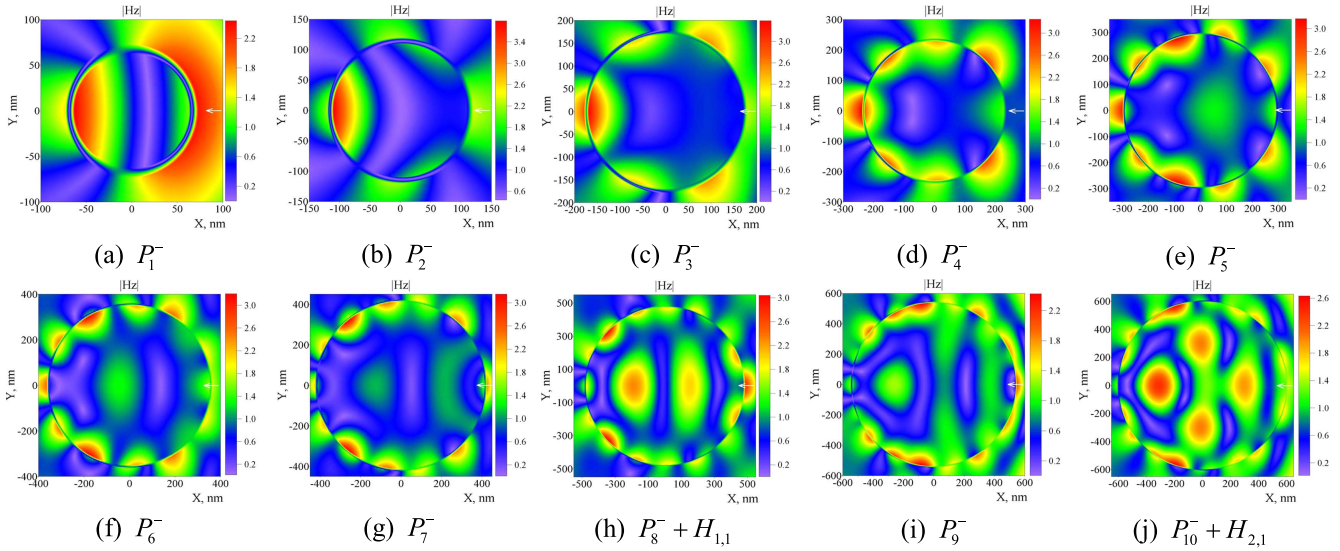

Figure 15. The near-zone magnetic field patterns in the ACS maxima for silver tube with the radius values $a = 73$ nm (a), 120 nm (b), 179 nm (c), 239 nm (d), 300 nm (e), 362 nm (f), 424 nm (g), 485 nm (h), 547 nm (i), 608 nm (j), all at the wavelength $\lambda = 600$ nm.

ORCID iDs

Elena A Velichko https://orcid.org/0000-0001-6018-1761

References

[1] Novotny L and Hecht B 2012 *Principles of Nano-Optics* (Cambridge: Cambridge University Press)
[2] Johnson P B and Christy R W 1972 Optical constants of the noble metals *Phys. Rev.* B **6** 4370
[3] Lukyanchuk B S and Ternovsky V 2006 Light scattering by a thin wire with a surface-plasmon resonance: bifurcations of the poynting vector field *Phys. Rev.* B **73** 235432
[4] Anyutin A P, Korshunov I P and Shatrov A D 2015 On the influence of the medium loss on resonances of surface plasmons in a cylinder *J. Commun. Tech. Electron.* **60** 572
[5] Moroz A 2010 Non-radiative decay of a dipole emitter close to a metallic nanoparticle: importance of higher-order multipole contributions *Opt. Comm.* **283** 2277
[6] Andrianov E S, Pukhov A A, Vinogradov A P, Dorofeenko A V and Lisyansky A A 2014 Spontaneous radiation of a two-level atom into multipole modes of a plasmonic nanoparticle *Photonics Nanostruct.* **12** 387
[7] Kolwas K and Derkachova A 2013 Damping rates of surface plasmons for particles of size from nano- to micrometers; reduction of the nonradiative decay *J. Quant. Spectrosc. Radiat. Transfer* **114** 45
[8] Wiederrecht G P 2004 Near-field optical imaging of noble metal nanoparticles *Eur. Phys. J. Appl. Phys.* **28** 3–18
[9] Esteban R, Vogelgesang R, Dorfmuller J, Dmitriev A, Rookstuhl C, Etrich C and Kern K 2008 Direct near-field optical imaging of higher order plasmonic resonances *Nano Lett.* **8** 3155–9
[10] Kong D, Jiang L and Drucker J 2015 Interpreting plasmonic response of epitaxial Ag/Si (100) island ensembles *J. Appl. Phys.* **118** 213103
[11] Prodan E, Radloff C, Halas N J and Nordlander P 2003 A hybridization model for the plasmon response of complex nanostrustures *Science* **302** 419
[12] Zhu J 2007 Theoretical study of the light scattering from gold nanotubes: effect of wall thickness *Mater. Sci. Eng.* A **454** 685
[13] She H–Y, Li L-W, Martin O J F and Mosig J R 2008 Surface polaritons of small coated cylinders illuminated by normally incident TM and TE waves *Opt. Express* **16** 1007
[14] McMahon J M, Gray S K and Schatz G C 2010 Nonlocal dielectric effects in core–shell nanowires *J. Phys. Chem.* C **114** 15903
[15] Xu H, Li H, Liu Z, Xie S, Zhou X and Wu J 2011 Adjustable plasmon resonance in the coaxial gold nanotubes *Solid State Commun.* **151** 759
[16] Velichko E A and Nosich A I 2013 Refractive-index sensitivities of hybrid surface-plasmon resonances for a core–shell circular silver nanotube sensor *Opt. Lett.* **38** 4978
[17] Anyutin A P, Korshunov I P and Shatrov A D 2015 Plasmon resonances in a quartz nanofiber coated with a silver layer *J. Commun. Tech. Electron.* **60** 952
[18] Raze S, Toscano G, Jauho A-P, Mortensen N A and Wubs M 2013 Refractive-index sensing with ultrathin plasmonic nanotubes *Plasmonics* **8** 193
[19] Murphy A *et al* 2013 Fabrication and optical properties of large-scale arrays of gold nanocavities based on rod-in-a-tube coaxials *Appl. Phys. Lett.* **102** 103103
[20] Velichko E A Resonance scattering and absorption of light by a silver circular cylinder with diameter larger than the wavelength *Proc. Int. Conf. IEEE UKRCON-2017* (Kyiv) pp 663–6
[21] Strutt J W and (Lord Rayleigh after 1902) 1881 On the electromagnetic theory of light *Philos. Mag.* **12** 81
[22] Babar S and Weaver J H 2015 Optical constants of Cu, Ag, and Au revisited *Appl. Opt.* **54** 477
[23] Natarov D M 2014 Modes of a core–shell silver wire plasmonic nanolaser beyond the Drude formula *J. Opt.* **16** 075002
[24] Yang F, Sambles J R and Bradberry G W 1991 Long-range surface modes supported by thin films *Phys. Rev.* B **44** 5855
[25] Shapoval O V and Nosich A I 2013 Finite gratings of many thin silver nanostrips: optical resonances and role of periodicity *AIP Adv.* **3** 042120
[26] Zinenko T L, Marciniak M and Nosich A I 2013 Accurate analysis of light scattering and absorption by an infinite flat grating of thin silver nanostrips in free space using the method of analytical regularization *IEEE J. Sel. Top. Quant. Electron.* **19** 9000108
[27] Velichko E A and Nosich A I 2013 Hybrid plasmon resonances in the scattering and absorption of light by a circular silver nanotube *Proc. Int. Conf. Advanced Optoelectronics and Lasers (CAOL-2013)* (Sudak) p 229